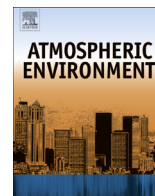


Contents lists available at [SciVerse ScienceDirect](http://www.sciencedirect.com)

# Atmospheric Environment

journal homepage: [www.elsevier.com/locate/atmosenv](http://www.elsevier.com/locate/atmosenv)

## Detection, variations and intercomparison of the planetary boundary layer depth from radiosonde, lidar and infrared spectrometer



Virginia Sawyer, Zhanqing Li\*

Dept. of Atmospheric &amp; Oceanic Sciences and ESSIC, University of Maryland, College Park, MD 20740, USA

### H I G H L I G H T S

- A new method for detecting planetary boundary layers is introduced.
- The method is valid for use with micropulse lidar, radiosonde and infrared spectrometer.
- PBLs spanning eight years are obtained and compared among different input data.
- Diurnal and seasonal variations of PBL are presented over the SGP of US.
- Strengths and limitations are revealed.

### A R T I C L E I N F O

#### Article history:

Received 4 March 2013

Received in revised form

21 June 2013

Accepted 10 July 2013

#### Keywords:

Planetary boundary layer

Aerosol

Lidar

Radiosonde

Boundary-layer depth

### A B S T R A C T

The depth of the planetary boundary layer (PBL) and its temporal evolution have important effects on weather, air quality and climate. While there are methods to detect the PBL depth from atmospheric profiles, few can be applied to different types of measurements and cope with changing atmospheric conditions. Many require supporting information from other instruments. In this study, two common methods for PBL depth detection (wavelet covariance and iterative curve-fitting) are combined, modified and applied to long-term time series of radiosonde profiles, micropulse lidar (MPL) measured backscatter and atmospheric emitted radiance interferometer (AERI) data collected at the Atmospheric Radiation Measurement (ARM) Southern Great Plains (SGP) site. Intercomparison among the three PBL retrieval products shows the robustness of the algorithm. The comparisons were made for different times of day, four seasons, and variable sky conditions. While considerable uncertainties exist in PBL detection using all three types of measurements, the agreement among the PBL products is promising under certain conditions, and the different measurements have complementary advantages. The best agreement in the seasonal cycle occurs in winter, and the best agreement in the diurnal cycle when the boundary-layer regime is mature and changes slowly. PBL depths from instruments with higher temporal resolution (MPL and AERI) are of comparable accuracy to radiosonde-derived PBL depths; AERI excels for shallow PBLs, MPL for cloudy conditions. The new continuous PBL data set can be used to improve model parameterizations of PBL and our understanding of atmospheric transport of pollutants which affect clouds, air quality and human health.

© 2013 Elsevier Ltd. All rights reserved.

## 1. Introduction

The planetary boundary layer (PBL) is the lowest layer of the troposphere, ranging from several hundred meters to a few kilometers in depth. Directly affected by surface conditions, it is distinguishable from the free troposphere by differences in flow, thermodynamic properties, and chemical content. The last of these

is critical to surface air quality (Seinfeld and Pandis, 2006) because the PBL depth determines a finite but varying volume into which pollutants can disperse. Over land, diurnal surface heating produces a clear cycle in the PBL depth (e.g., Liu and Liang, 2010), with convective boundary layers as high as 5 km possible under extreme conditions (Ma et al., 2011). If insolation stops during the day, as during the solar eclipse observed by Amiridis et al. (2007), the PBL top height decreases just as it typically does in the evening. Elsewhere, the PBL depends more strongly on synoptic conditions, but still changes significantly over time scales of hours.

The most common measurements of thermodynamic profiles are taken by radiosonde. These are launched twice a day operationally, or 4–8 times daily during field experiments (Seibert et al.,

\* Corresponding author. Present address: College of Global Change and Earth System Science, State Laboratory of Earth Surface Process and Resource Ecology, Beijing Normal University, PR China.

E-mail address: [zli@atmos.umd.edu](mailto:zli@atmos.umd.edu) (Z. Li).

2000). The temporal resolution in radiosonde-derived PBL data is therefore too sparse to detect the evolution of the diurnal structure. Smaller-scale boundary layer processes and waves are obscured. For many sites in the western hemisphere, operational radiosonde launches also occur during transition times when the PBL is changing rapidly (00UTC and 12UTC) so extremes of the diurnal cycle go unobserved. PBL detection by remote sensing can improve the temporal resolution of the data, usually by using a proxy for the thermodynamic profile. Wind profiling provides some clues about the turbulence structure, so radar wind profilers (Bianco and Wilczak, 2002) and sodars are used to detect the PBL (Beyrich and Górsdorf, 1995). Another useful measurement is the distribution of aerosol with height.

Because buoyant stability restricts the mixing of aerosols through the boundary layer top to special circumstances (Donnell et al., 2001; Twohy et al., 2002; Henne et al., 2004; Ding et al., 2009), the PBL top can be inferred from the vertical distribution of aerosols through the lower troposphere, using aerosol as a tracer. A well-mixed boundary layer has a fairly uniform aerosol concentration with height, and is also more polluted than the free troposphere (Melfi et al., 1985). The MPL backscatter signal in the PBL is accordingly stronger and more uniform with altitude than the signal in the free troposphere. Boundary layer clouds, which return stronger backscatter signals, can also help determine the depth of the PBL (Davis et al., 2000). Several “gradient” methods rely on the drop in aerosol concentration across the boundary in order to detect the PBL top height, defined as the center of a transition zone or inversion at the top of the surface layer.

This study presents an improved algorithm for determining the depth of the PBL. This method uses data collected from 1996 to 2004 at the Department of Energy’s Atmospheric Radiation Measurement Southern Great Plains (SGP) site. Two gradient methods typically used to determine the PBL depth are described in Section 2. They are combined to obtain a new algorithm. Datasets to which this algorithm was applied are described in Section 3. Section 4 presents comparisons of PBL depths derived from data acquired by different instruments and diurnal/seasonal variations in PBL depth. A discussion and summary follow.

## 2. Methodology

### 2.1. Gradient methods

Simple gradient methods for PBL detection involve threshold values for mixed-layer lidar backscatter signals (Melfi et al., 1985; Palm et al., 1998) or the first derivative of the lidar backscatter signal (Amiridis et al., 2007). These are effective for short-term, relatively uniform data sets, but they require too much prior knowledge of instrument properties and atmospheric conditions to be suitable for automation. Edge detection software in programs such as Photoshop can also detect layers in lidar backscatter (Parikh and Parikh, 2002).

A more sophisticated and commonly used method involves the wavelet covariance transform (Davis et al., 2000; Brooks, 2003). It allows comparison between the backscatter sounding and the Haar wavelet, which is defined as

$$\left(\frac{z-b}{a}\right) = \begin{cases} -1 & : b - \frac{a}{2} \leq z \leq b \\ 1 & : b \leq z \leq b + \frac{a}{2}, \\ 0 & : \text{elsewhere} \end{cases} \quad (1)$$

where  $a$  is the dilation of the Haar wavelet,  $b$  is the translation of the Haar wavelet, and  $z$  is the altitude. The wavelet covariance transform,  $W_f(a, b)$ , is expressed as

$$W_f(a, b) = a^{-1} \int_{zb}^{zt} f(z)h\left(\frac{z-b}{a}\right) dz, \quad (2)$$

where  $f(z)$  is the backscatter sounding. The function  $W_f(a, b)$  reaches its maximum value when  $b$  reaches the strongest negative gradient in the backscatter with height, i.e. the top of the PBL. In Equations (1) and (2),  $a$ , the dilation of the Haar wavelet, corresponds physically to the depth of the entrainment zone. It is possible, but computationally intensive, to repeat the algorithm while varying  $a$  to find its optimal value. The PBL is given as the center of a transition zone defined by the width of the dilation. For very small values of  $a$  the algorithm detects noisy PBL depths because of spurious gradients; for very large values, the detected PBL is too high. In the middle, however, is a wide range of  $a$  values for which the algorithm plateaus at the correct PBL depth (Fig. 1). The entrainment zone depth (EZD) is the smallest value of  $a$  capable of finding the plateau PBL depth (Brooks, 2003). However, a constant dilation value can be used as long as it falls within the plateau range for most profiles. In this study,  $a$  is held constant at 1 km.

The wavelet covariance transform requires little prior information about the atmosphere or the lidar, and works equally well with data from several instrument types. This makes the algorithm useful for automated PBL detection in multiple data sets. It is independent of absolute backscatter values as long as the signal-to-noise ratio is high enough to distinguish the PBL. However, bright backscatter signals from high clouds and elevated aerosol plumes can sometimes overshadow the signal from the PBL, causing an elevated bias in PBL detection. A solution is to limit the vertical extent of the backscatter profile to which the algorithm is applied. While the full vertical profile for lidar backscatter extends tens of kilometers into the atmosphere, the PBL does not occur beyond the low troposphere; a limit on the algorithm of 3 km is suitable for most sites. This also reduces the computing time.

Steyn et al. (1999) developed a different algorithm for PBL detection in the lidar backscatter gradient. To avoid the problems

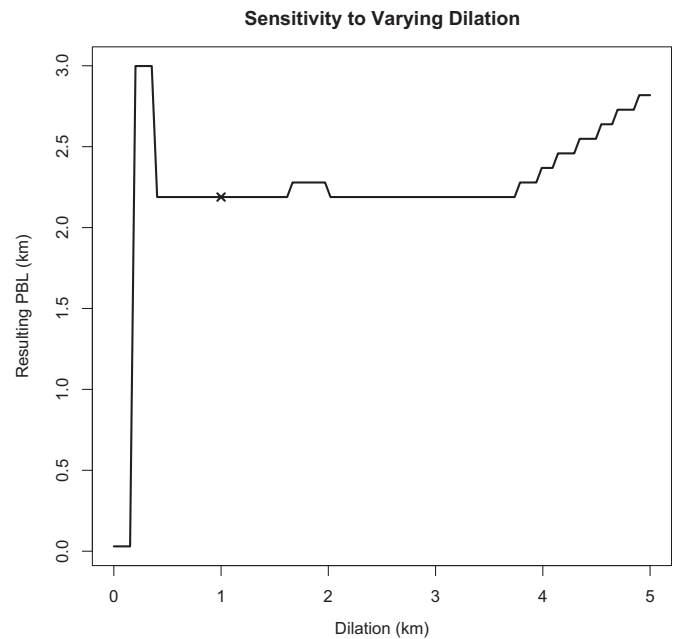


Fig. 1. Wavelet covariance-detected PBL depths from a single lidar backscatter profile (21:00 UTC Aug. 15, 2003, at the SGP site) using varying values of the Haar dilation  $a$ . The EZD is 400 m deep, but the assumed 1 km dilation (crossed) is within the plateau range.

posed by multiple bright features in the backscatter, the algorithm uses the shape of a curve representing an idealized backscatter profile, namely,

$$B(z) = \frac{(B_m + B_u)}{2} - \frac{(B_m - B_u)}{2} \operatorname{erf}\left(\frac{z - z_m}{s}\right). \quad (3)$$

Here,  $B_m$  and  $B_u$  are the backscatter values for the mixed layer and the lower free troposphere, respectively,  $z_m$  is the depth of the PBL, and  $s$  is a parameter defining the depth of the sigmoid curve between  $B_m$  and  $B_u$ . As before,  $z_m$  is defined as the center of a transition zone, which in this case has a depth equal to 2.77 times the value of  $s$ , assuming as in Steyn et al. (1999) that the entrainment zone encompasses 95% of the depth of the curve. The algorithm solves for these four parameters simultaneously to minimize the root-mean-square difference between the idealized curve and the backscatter sounding. As such, it arrives at an estimate of the transition, or EZD, as well as the PBL depth. Simulated annealing, as detailed by Press et al. (1992), is a robust method for fitting the curve; the fit improves with the quality of the initial guess. Steyn et al. (1999) used the algorithm with airborne lidar data, which necessarily operates for short periods of time alongside other instruments. For longer-term, ground-based deployments, no single initial guess is appropriate for the entire time series.

The simulated annealing routine escapes from local minima and troughs that would trap a downhill simplex routine because it introduces a small random element to the solution (Press et al., 1992). It can therefore find multiple solutions given the same input. Over a time series in which the PBL changes slowly compared to the measurement interval, PBL returns from a simulated annealing algorithm appear “noisy”, with unrealistically abrupt changes in height. Hägeli et al. (2000) details the appropriate interval for a running-mean filter, based on the dimensions of the data and the estimated vertical motion at the boundary layer top. For a stationary lidar deployment, a 25-min interval matches the scale of the boundary-layer turbulence. With smoothing, the Steyn et al. (1999) algorithm is more sensitive to small-scale boundary layer waves than the wavelet covariance transform. Because curve-fitting uses the whole backscatter signal as a single shape, it also tolerates more extraneous features and noise.

Ground-based MPL cannot retrieve backscatter near the surface. Regardless of algorithm, shallow PBLs are sometimes missed, and residual layers are detected instead.

## 2.2. The combined algorithm

The advantages and disadvantages of the two gradient methods suggest that PBL depth detection might be improved by using both in combination. The wavelet covariance transform is suitable alone for automated PBL detection, but it can also generate a first guess for the simulated annealing routine. The backscatter values for the free troposphere and the mixed layer are the mean backscatter values above and below the first-guess PBL, respectively, and the EZD is the 1 km assumed by the wavelet covariance transform. In turn, the curve-fitting process refines the PBL solution so that it is less sensitive to elevated cloud and aerosol layers and more sensitive to changes in the boundary layer depth, while simultaneously solving for the depth of the aerosol transition. The resulting two-step process (Fig. 2) remains simple enough for the computational limitations of long-term automated analysis. The algorithm considers each backscatter profile separately until the final step, in which the running-mean filter suggested by Hägeli et al. (2000) is applied. Fig. 3 illustrates how this smooths the PBL time series to eliminate random jumps introduced by the simulated annealing process. PBL depths are detected at a 5-min resolution, so the 25-min smoothing interval is a five-cell filter. The details of small-scale waves within the boundary layer top are preserved in the final time series.

With modification, the same algorithm can be applied to thermodynamic profiles from radiosondes and ground-based remote sensing. This eliminates discrepancies introduced by using a different algorithm, such as what Liu and Liang (2010) developed. Defining the PBL as before—the center of an inversion in the virtual potential temperature ( $\theta_v$ ) profile (Stull, 1988)—the algorithm must detect a sharp increase in  $\theta_v$  with height between the nearly-uniform mixed layer and the more stable free troposphere above. This means that the wavelet covariance part of the algorithm must use the negative of Equation (1), that is

$$\left(\frac{z-b}{a}\right) = \begin{cases} 1 & : \quad b - \frac{a}{2} \leq z \leq b \\ -1 & : \quad b \leq z \leq b + \frac{a}{2} \\ 0 & : \quad \text{elsewhere} \end{cases}$$

Care must be taken to exclude the tropopause from analysis, but it seldom appears at altitudes where the PBL might be expected. In addition, the thermodynamic profile as a whole is often too stable for the algorithm to distinguish inversions. It performs more reliably if the linear regression of the lowest few kilometers is

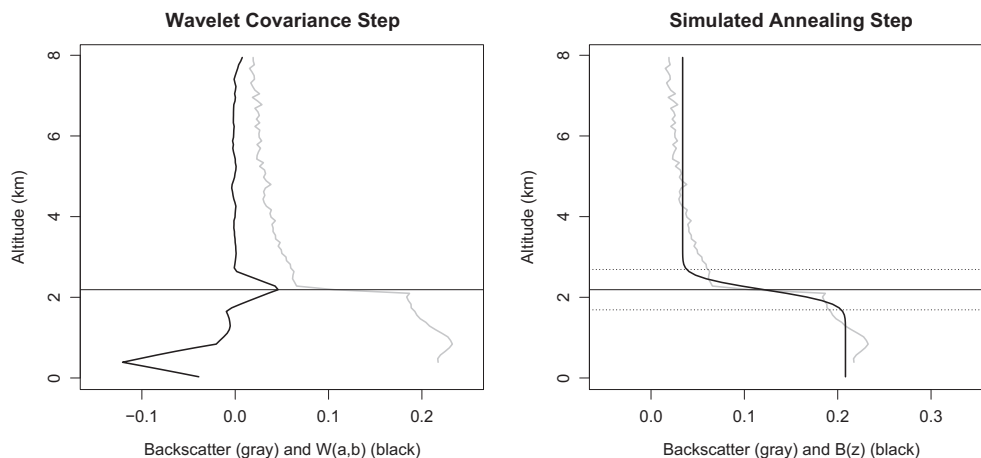


Fig. 2. The combined PBL detection algorithm applied to a single backscatter profile, taken 21:00 UTC Aug. 15, 2003 at the SGP site. The solid horizontal line is the PBL depth detected by two steps of the combined algorithm. The dotted lines show the limits of the EZD.

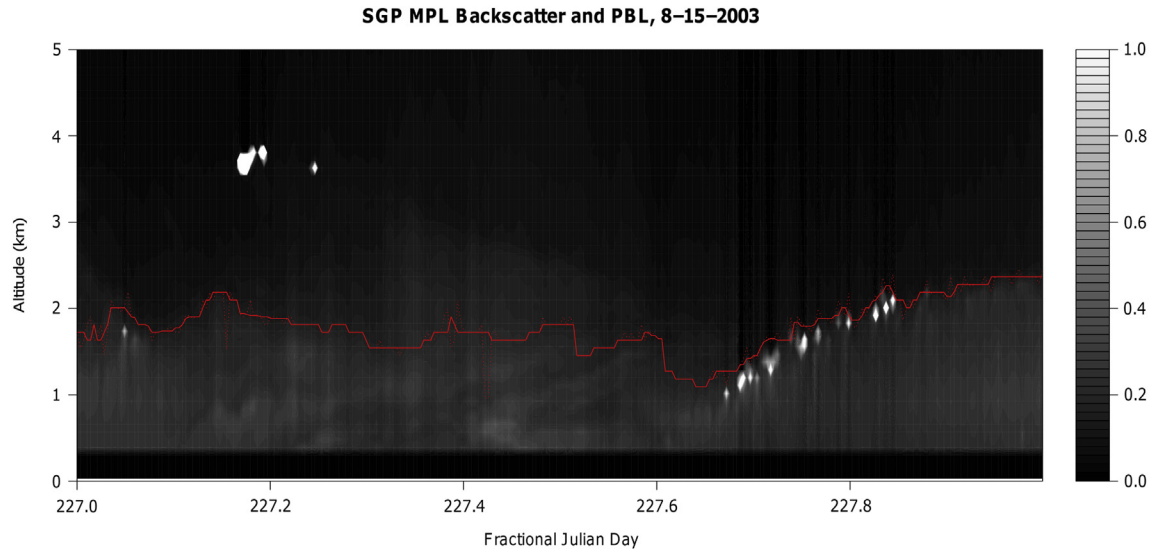


Fig. 3. Aug. 15, 2003 at SGP. The dotted line indicates the PBL detected by the combined algorithm before smoothing; the solid line applies the running-median filter.

subtracted from the profile, so that the detection algorithm analyzes deviations from the mean lapse rate. Then the curve-fitting process can refine the first guess and estimate the EZD as before.

### 3. Datasets used

#### 3.1. Micropulse lidar (MPL)

This study uses an MPL backscatter time series collected at the SGP site near Ponca City, OK (36°36'18.0" N, 97°29'6.0" W). The dataset begins in May 1996 and is analyzed through 2004, with some gaps and instrument reconfigurations during the eight years. The lidar uses a single wavelength at 532 nm. Signal is corrected for instrument artifacts (background, afterpulse, deadtime, overlap, and range normalization) but not for aerosol extinction. Backscatter profiles have a vertical resolution of 75 m and are taken once every minute, but the PBL is detected at five-minute intervals. As a ground-based, upward-directed configuration, the MPL returns backscatter within a vertical range that begins approximately 600 m above the surface and extends, when not attenuated by cloud cover, to more than 30 km. The lowest 600 m are not accurately measured because of incomplete overlap between the laser beam spread and the telescope field of view; signal from the upper atmosphere is subject to interference from sunlight and attenuation of the laser pulse. In May 2004 the lidar was upgraded with a depolarization switch, which may affect results. Measurements after that time are not included in this study.

#### 3.2. Thermodynamic profiles from radiosonde and AERI

Radiosonde launches took place at least four times per day at the SGP site, not always only at the usual 00:00, 6:00, 12:00, and 18:00 UTC. There are smaller, but still considerable, numbers of measurements for 3:00, 9:00, 15:00, and 21:00 UTC. Enough launches took place at this second set of times that the diurnal cycle of PBL depths can be analyzed at 3-h intervals, even though no individual day had all eight measurements taken. Individual vertical profiles of  $\theta_v$  were analyzed for PBL depth and EZD using the modified algorithm introduced in this study, but the smoothing step is omitted due to the longer time between measurements. Vertical resolutions for radiosonde launches vary according to the balloon ascent rate, but data points occur approximately 10 m apart.

The SGP site also hosts an *atmospheric emitted radiance interferometer* (AERI), which retrieves one  $\theta_v$  profile every eight minutes (Feltz et al., 1998, 2003); a three-cell running-mean filter comes close to the 25-min target interval. However, the vertical resolution decreases with height.  $\theta_v$  is retrieved every 50 m at the surface but by 500 m, retrievals are made at 500-m intervals. At the top of the profile, the resolution is 2 km. In addition, cloudy profiles must be excluded. AERI retrievals are available from June 1996 to the present, with a change to the data format in 2002.

In both campaign and SGP datasets, radiosonde-derived PBL depths are matched to the equivalent lidar-derived and AERI-derived PBLs by averaging the lidar and AERI results over the 20 min following the launch of the radiosonde: the mean of four consecutive lidar-derived PBL depths, or 2–3 PBL depths from AERI. This allows time for the balloon's ascent. Because the  $\theta_v$  profiles from radiosonde and AERI are used in comparison with MPL, the data period analyzed for all three instruments is May 1996 to May 2004.

### 4. Results

#### 4.1. Intercomparison of PBL depth detection

The algorithm is evaluated by comparing PBL results from each instrument against one another. Because they are from the same site, their time series are matched to one another and the PBL depth detection uses the same algorithm, the comparison minimizes variables. In the case of AERI vs. radiosonde (Fig. 4), the measurements are two sets of thermodynamic profiles; the differences in PBL depth come from differences in instrument precision and resolution. Because neither method is considered true, an orthogonal regression is used instead of a simple linear fit. Two-thirds of the variation is accounted for ( $R^2 = 0.681$ ). Most points lie close to the 1:1 line. While the regression is influenced by a cluster of results in which the radiosonde-derived PBL depth is much higher than the AERI-derived PBL depth, the overall systematic error is low. Much of the correspondence with AERI data is only achieved using the combined algorithm, because the low vertical resolution of the AERI-derived thermodynamic profiles strongly affects the wavelet covariance transform.

For comparison between radiosonde and MPL-derived PBL depths, it is important to assure that clouds do not interfere with

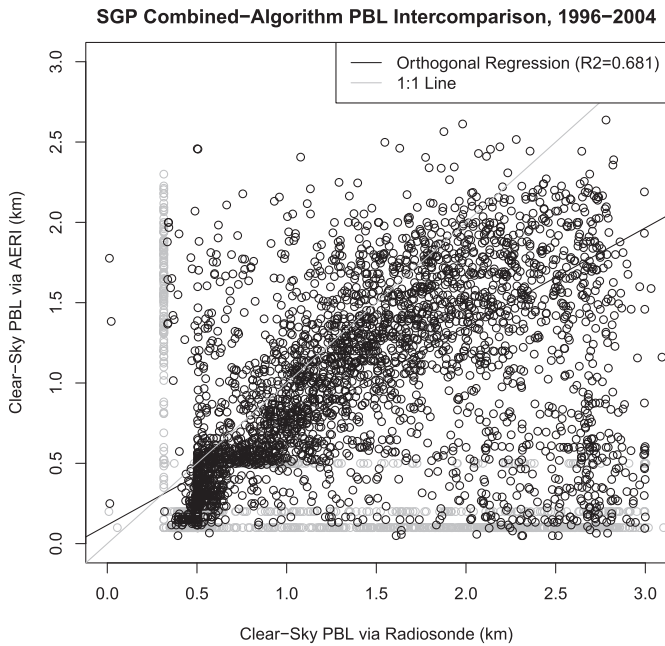


**Fig. 4.** Comparison between AERI- and radiosonde-derived PBL depths at SGP. After the removal of artifacts indicating weak signal (gray points), the orthogonal regression is  $PBL_{AERI} = 0.62PBL_{sonde} + 0.12$ .

PBL detection (Fig. 5). Clouds return bright backscatter at the lidar wavelength, and the attenuation of the laser pulse through an optically thick cloud deck appears as a sharp backscatter gradient that may be targeted by the PBL detection algorithm. The wavelet covariance transform component of the PBL detection algorithm is restricted to 3 km from the surface, partly because the PBL typically occurs there (Stull, 1988; see Ma et al., 2011 for a rare exception), but partly to eliminate interference by higher-altitude clouds. However, most low-level cloud bases occur at or near the PBL, either because the capping inversion prevents stratocumulus clouds from developing farther or because the cloud base in a deep convective cell marks the PBL top (Stull, 1988). The algorithm therefore returns an answer about as accurate as it would have from aerosol backscatter alone.

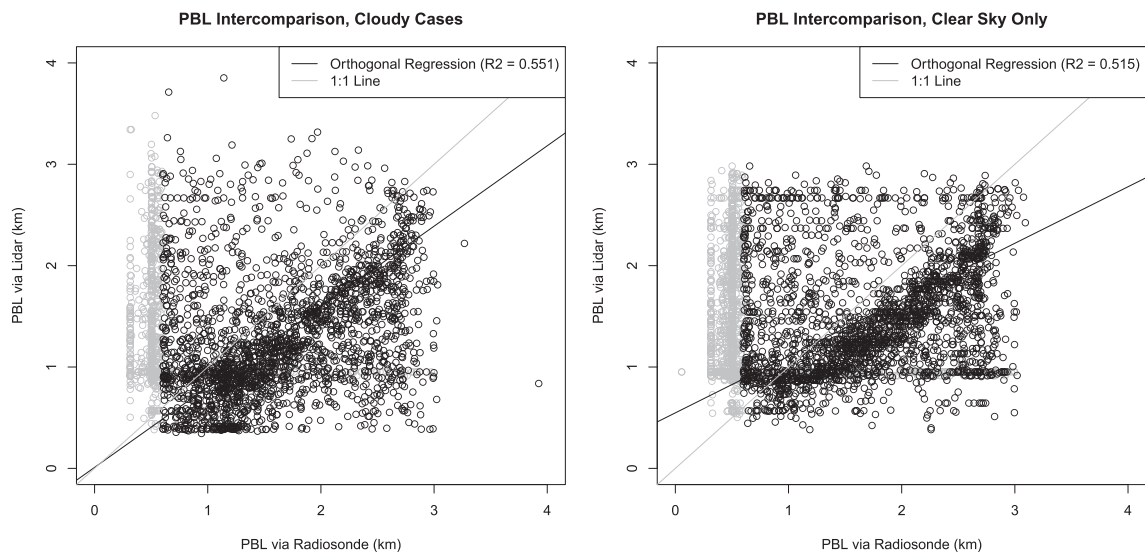


**Fig. 5.** Radiosonde- vs. MPL-derived PBL depths at SGP, cloudy cases (left) and cloud-free cases (right).  $R^2$  values for the orthogonal regression are 0.551 and 0.515, respectively. Gray points, excluded from regression, are outside the lidar overlap range.

In all MPL-derived PBL depths, the incomplete overlap between the laser beam spread and the telescope field of view imposes a lower limit on the instrument range. Radiosonde-derived PBL results below 600 m (27% of cases) are excluded from regression because the lidar cannot observe them, although radiosonde can. There is little difference between cloudy and cloud-free lidar PBL detection, however. The following intercomparison therefore uses the full set of results (Fig. 6).

#### 4.2. Diurnal cycles

Although the lidar-derived PBL depths are matched to radiosonde launch times, the comparison does not discriminate between day and nighttime observations. Continental boundary layers undergo strong diurnal cycling through regimes (Fig. 7), classified according to whether the surface undergoes radiative heating (daytime) or cooling (night). Fig. 8 shows that as expected (e.g., Stull 1988) the PBL top depth as detected by radiosondes over the continental SGP site has its minimum in the early morning and its maximum coinciding with peak convection in the afternoon. Lidar-derived PBL top heights show a cycle of the same phase, but smaller amplitude. The cosine curve fitted to the median radiosonde-derived PBL depth with time has an amplitude of 470 m and an  $R^2$  value of 0.97. For MPL-derived PBL depths, the amplitude is only 170 m and the  $R^2$  is 0.85. This may happen because the aerosol distribution through the column does not follow the thermodynamic profile exactly, especially during times of transition. In addition, some times of day allow for more accurate MPL-based PBL detection than others. This is especially true because nocturnal stable boundary layers are often shallow enough to fall below the lidar overlap range.

The AERI-derived PBL depths show a similar cycle (Fig. 9) to the radiosonde-derived PBL, with shallow PBLs included in the analysis. While the MPL overlap range limits its ability to observe lower altitudes, the AERI profile improves near the surface. Because the vertical resolution of the instrument decreases with height, it can detect shallow PBL depths with greater precision than deeper PBLs. The results that can be compared to MPL-derived PBL depths, i.e. those that occur above the overlap range limit, are less reliable than the shallower AERI-derived PBL depths that can be compared only to radiosonde. Consequently, the relationship between AERI-

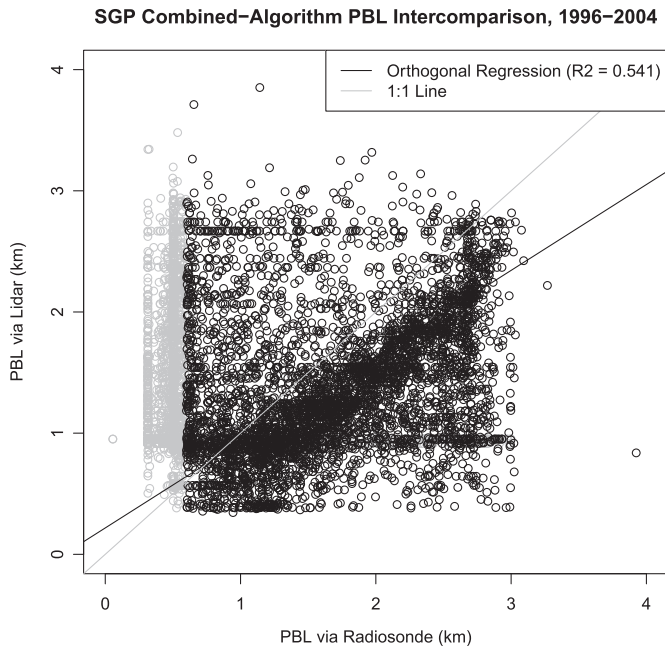


**Fig. 6.** Intercomparison between all radiosonde- and MPL-derived PBL depths at SGP. The orthogonal regression is  $PBL_{MPL} = 0.71PBL_{sonde} + 0.22$ . Gray points, excluded from regression, are outside the lidar overlap range.

derived and MPL-derived PBL depths is not strong enough for a meaningful comparison of the diurnal cycle. It makes more sense to compare the AERI-derived PBL diurnal cycle to that of radiosonde, this time with shallow PBL depths from both instruments included. The amplitude of the cosine regression expands to 660 m for radiosonde results ( $R^2 = 0.90$ ). For AERI-derived PBL depths, the amplitude is 440 m and the  $R^2$  value is 0.64. Because the strengths and limitations of the PBL products complement each other, all the products are valuable despite their inconsistency.

The agreement of PBL detection by the three methods varies with the time of day as seen in Fig. 10. Note that  $R^2$  values do not fall between zero and one. To prevent any systematic error specific to one time interval from appearing as misleading high agreement,  $R^2$  is always evaluated for the 1:1 line, i.e. perfect agreement between the two instruments, instead of the linear regression for each time

interval. Daytime PBL top heights show closer agreement between instruments than nighttime PBL top heights, and mature boundary layers, whether stable or convective, show more agreement than boundary layers that have just begun to collapse or develop. This may be partly because the radiosonde takes time to ascend, and the more snapshot-like profiles from MPL and AERI cannot match it exactly. Slowly changing PBL tops naturally make the best match. However, in the lidar, the same effect could also be due to pollutants that remain aloft in the residual layer when the convective boundary layer collapses, or that entrain downward into the growing convective boundary layer in the morning. Nocturnal stable boundary layers are more difficult to detect because the stability of that regime allows aerosols to form thin stratified layers instead of mixing uniformly. MPL-derived PBL depths show a greater influence of boundary layer maturity on the agreement with radiosonde than do AERI-derived PBL depths. This supports the idea that the vertical aerosol distribution does not change at exactly the same rate as  $\theta_v$ , and the use of MPL backscatter as a proxy for thermodynamic structure has some limitations.

#### 4.3. Seasonal cycles

The seasonal cycle of the PBL depth is as important as the diurnal cycle to mixed layer processes. Surface convection is stronger in the summer months than in the winter at continental sites, and the PBL top depth responds accordingly. Again the radiosonde results follow a cosine curve, its peak coinciding with the most intense surface heating. The difference in wave amplitude between the radiosonde- and MPL-based PBL top heights is still present but less pronounced (Fig. 11). The cosine curve fitted to the radiosonde-derived median values has an amplitude of 380 m and an  $R^2$  value of 0.93, while the cosine curve fitted to the MPL-derived median values has an amplitude of 330 m and an  $R^2$  value of 0.90. The radiosonde-derived PBL top heights average slightly higher and are more variable within any given month. This is consistent with the greater amplitude of the diurnal cycle shown in Fig. 6.

It seems counterintuitive, given that convective PBLs are analyzed more accurately than stable nocturnal boundary layers, that the instruments diverge most in the summer months (Fig. 12). For the diurnal cycle analysis, the highest PBL tops have the best agreement between the two instruments. For the seasonal cycle, they have the least, despite the fact that the MPL-derived seasonal

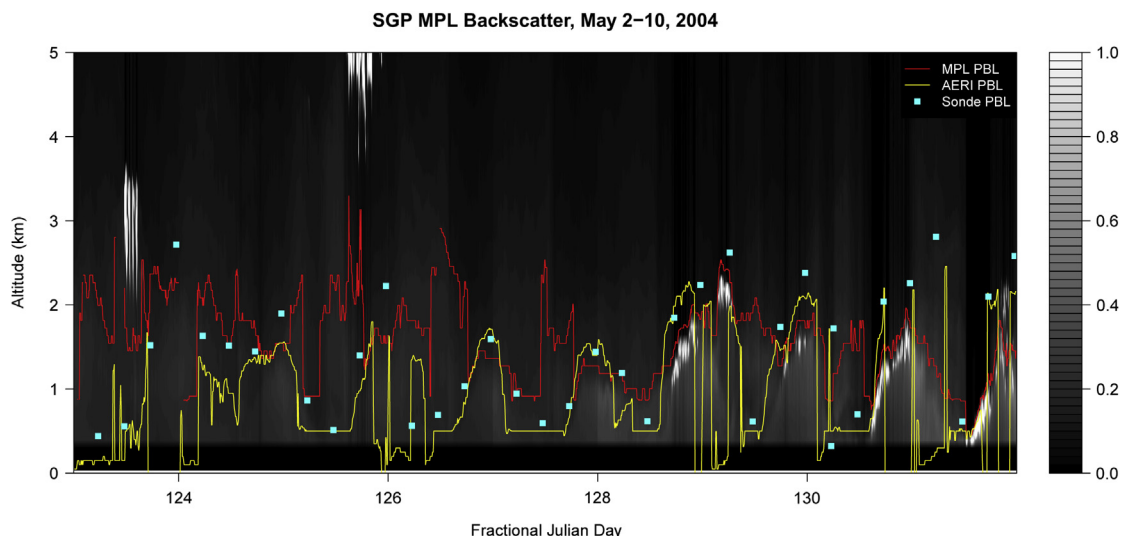


**Fig. 7.** PBL heights detected by MPL, AERI and radiosonde, overlaid on MPL backscatter during a nine-day period of typical conditions.

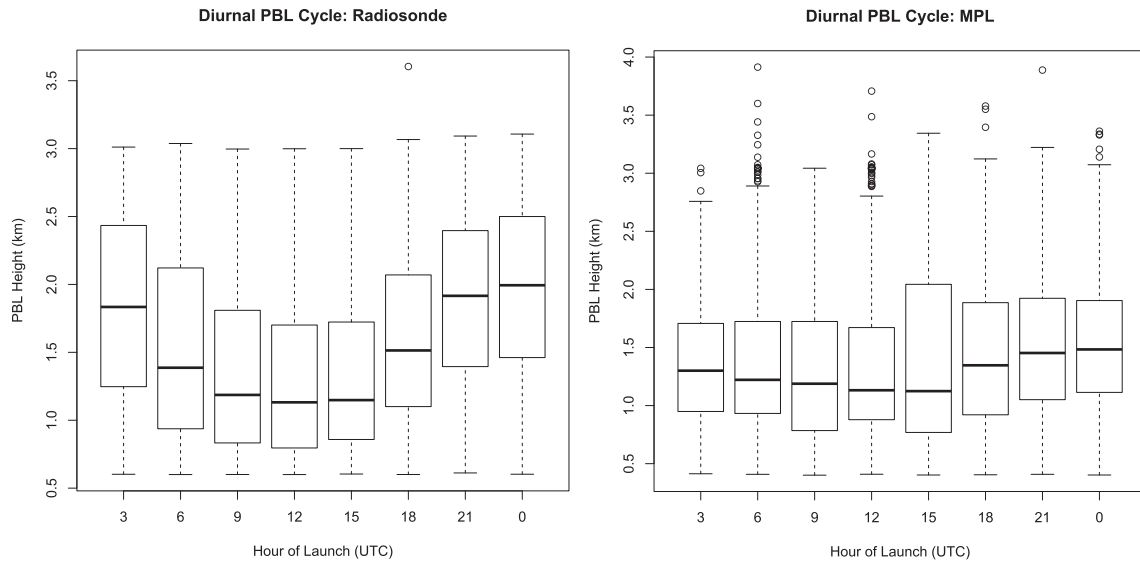


**Fig. 8.** Boxplots show the distribution of PBL depths from different radiosonde launch times by radiosonde (left) and MPL (right), excluding PBL depths outside the lidar overlap range.

cycle of PBL depths more closely resembles a cosine curve than the MPL-derived diurnal cycle. R-squared values vary to almost exactly the same degree as they do for the diurnal cycle shown in Fig. 9, but this time there is a steep drop in the quality of fit in the summer and a peak in the winter months.

The difference between the seasonal cycles in Fig. 11 appears mostly in the higher summertime PBL depths detected by radiosonde than by MPL, and this is a clue as to its cause. The reason for the discrepancy appears to be the effect of deep convection on the thermodynamic structure of the middle troposphere. Fig. 13 shows the seasonal variation of MPL-retrieved cloud base heights occurring at altitudes typical of boundary-layer clouds. The seasonal cycle peaks with a median cloud base height of approximately 1500 m in August, similar to the seasonal peak for the MPL-derived PBL depths. The radiosonde-derived PBL depths for the summer months are typically higher, and vary more. Although a schematic of PBL regimes in Medeiros et al. (2005) puts the PBL near the cloud

base in cases of deep convection, the convective turbulence fueled by surface heating extends all the way to the cloud top, which may well reach the tropopause during the kind of deep convection that is typical of summer in the Southern Great Plains. Temperature and moisture properties are similarly carried upward into the cloud. This renders the thermodynamic definition of the PBL ambiguous, and in such cases, the MPL may be more accurate than radiosondes as a PBL detection tool.

Because the  $\theta_v$  profiles from AERI and radiosonde have no overlap limitations, the comparison between AERI-derived and radiosonde-derived PBL depths is made without removing shallow PBLs (Fig. 14). Both radiosonde and AERI show a high frequency of shallow PBL depths in July and August, which makes it impossible to fit a cosine curve to the seasonal variation. The AERI-derived and radiosonde-derived PBL seasonal cycles show a few similarities to one another: their PBL depths peak in May and June and trough in December and January. However, the radiosonde-derived PBL

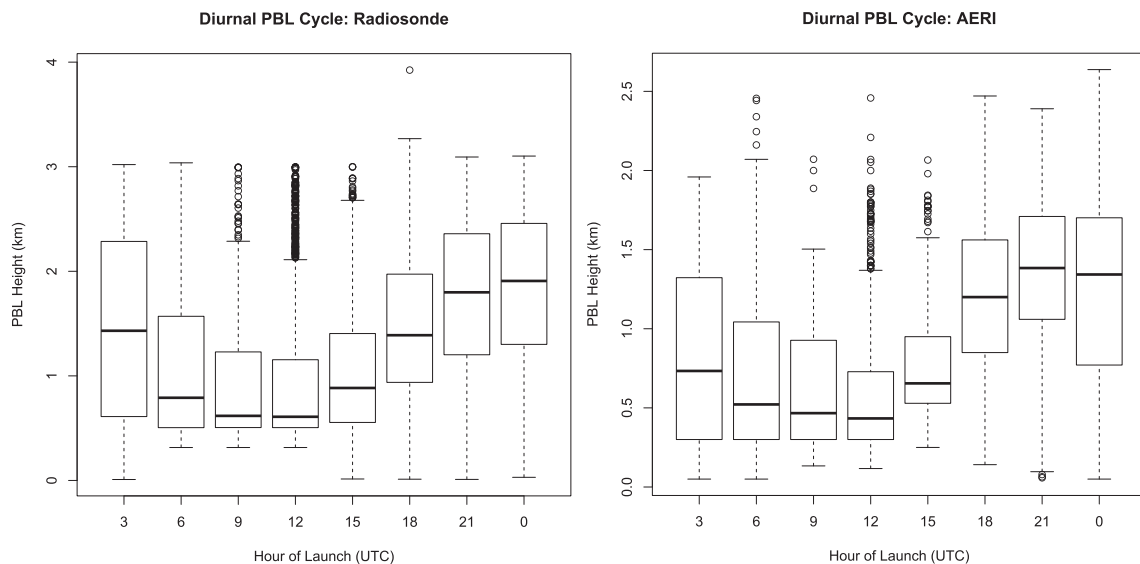


**Fig. 9.** Diurnal variations of PBL depth from radiosonde (left) and AERI (right).

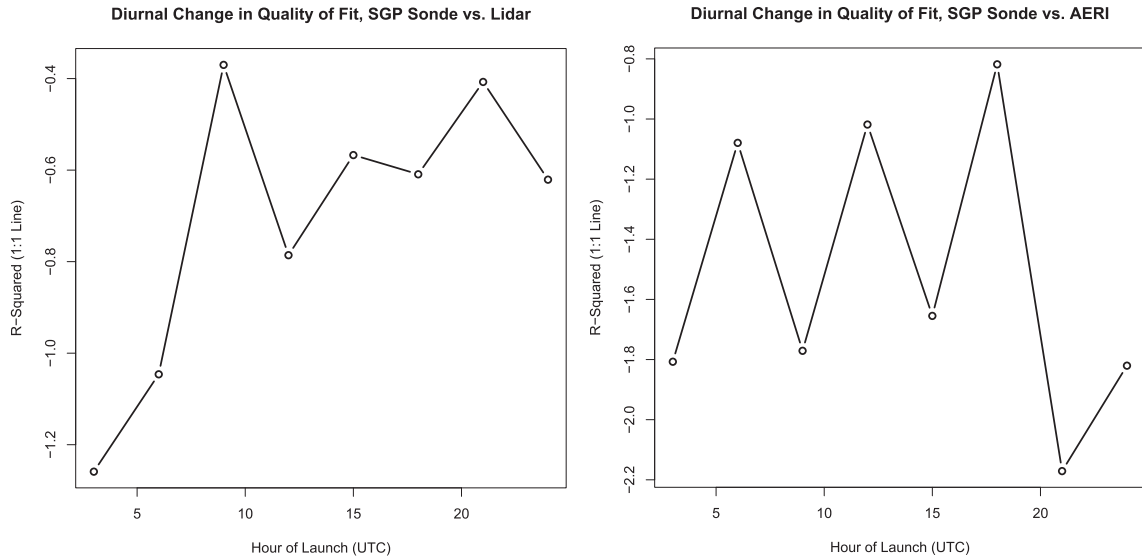


Fig. 10. Variation of  $R^2$  values with the time of radiosonde launches, assessing the quality of fit between  $PBL_{MPL}$  and  $PBL_{sonde}$  (left) and between  $PBL_{AERI}$  and  $PBL_{sonde}$  (right).

depths average higher in altitude than the AERI-derived PBL depths. The cluster of noncorresponding points in Fig. 3 affects the overall seasonal cycle. As with the MPL results, the agreement between AERI and radiosonde drops in the summer months (Fig. 15). Again, this is because the radiosonde-derived PBL depths are higher; the AERI-derived PBL depths for July and August have medians well below the MPL overlap limits, and vary less. This is in error, since unbroken stretches of low-level temperature inversions are associated with cold weather rather than the convective Great Plains summer. However, because of the variable vertical resolution of the instrument, ambiguous thermodynamic profiles—as in deep convection—may result in lower average PBL depths from AERI.

5. Discussion

The agreement between MPL and radiosonde in the presence of boundary-layer clouds (Fig. 4) conforms to expectations about boundary-layer stratocumulus, for which the cloud thickness remains shallow due to the PBL top acting as a capping inversion. This

is one of several boundary-layer regimes discussed in Medeiros et al. (2005), which also notes two complications. The first is decoupling of the flow within the stratocumulus deck from the rest of the mixed layer. Decoupling does not imply an additional temperature inversion, but is mostly apparent in measurements capable of profiling vertical motion, including wind lidar. Decoupling within a cloud layer does not appear in thermodynamic profiles, and to lidar it is hidden by the opacity of the cloud. The second complication is the possibility of a low stable boundary layer forming well below the level of the lowest cloud base. The wavelet covariance transform may then miss the signal of the PBL top because of the much stronger gradient caused by cloud attenuation. The combined algorithm avoids this problem by restricting the depth of the profile used in analysis, but may still err if the PBL is shallow and the elevated cloud base occurs at an altitude reasonable for PBL depths. Lastly, lidar cannot distinguish between shallow stratocumulus and deep cumulus convection, although both are distinct from other cloud types. The PBL is detected where the backscatter signal fully attenuates, which is slightly too high for

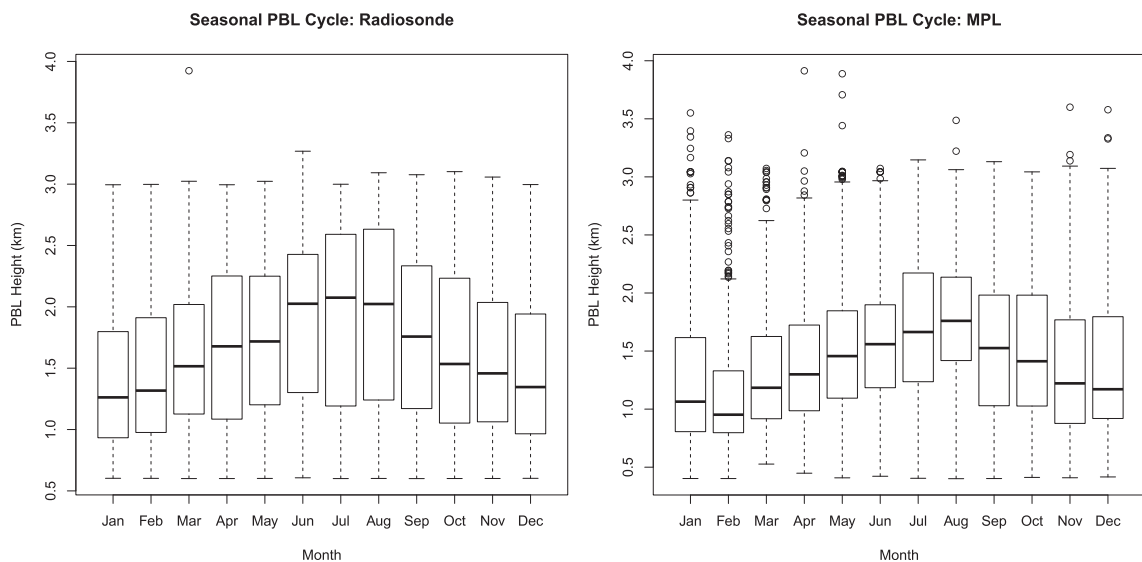


Fig. 11. Boxplots show the distribution of radiosonde-derived and MPL-derived PBL depths by month, with shallow PBLs excluded from the radiosonde record.

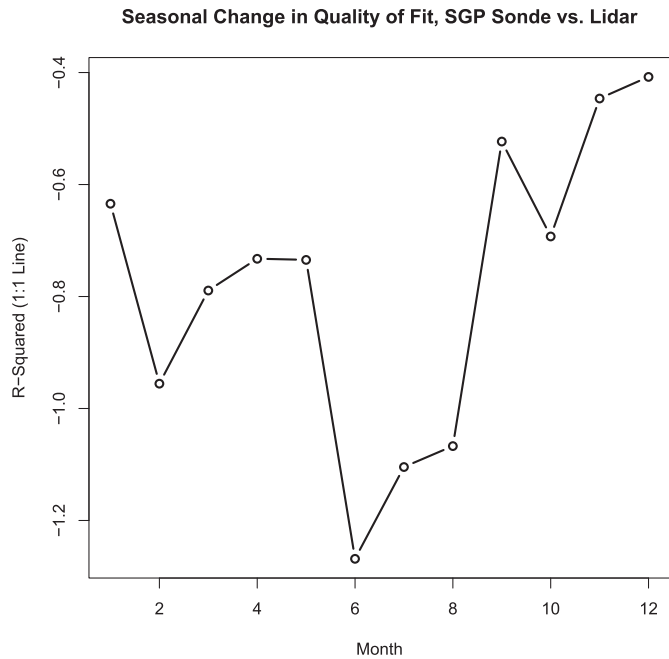


Fig. 12.  $R^2$  values assessing the quality of fit to the 1:1 line for the radiosonde-vs.-MPL intercomparison by month.

deep convection and slightly too low for a capping inversion over stratocumulus.

Steyn et al. (1999) recommends the simulated annealing routine partly because it finds the EZD, used to estimate fluxes through the boundary layer top. However, in the SGP results the detected EZD values hardly deviate from the constant initial guess, making EZD intercomparison among the different instruments impossible. A varying initial guess for the EZD, as there is for the PBL, would produce better results. However, wavelet covariance-based determination of the EZD is only possible by trial-and-error repetition

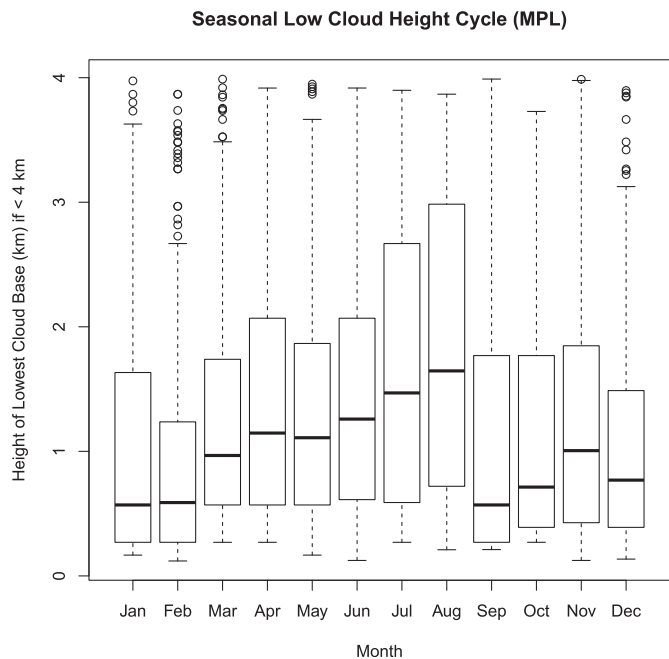


Fig. 13. Boxplots show the monthly distribution of MPL-retrieved cloud base depths located below 4 km at the SGP site for the period 1996–2004.

with different values of the wavelet dilation, a computationally intensive process. The transition between mixed-layer aerosol loading and the cleaner free troposphere may also have a different depth than the potential temperature inversion; aerosol content need not be as good a proxy for the transition as it is for the PBL. If this were the only obstacle, however, some relationship between radiosonde- and AERI-derived EZD results would be expected. None is found. EZD obtained by the combined algorithm is therefore unreliable, not suited to flux estimates.

For PBL detection, however, the benefit of the simulated annealing step is clear. Much of the correspondence in the AERI-derived PBL depth set is due to the use of the combined algorithm. Because the wavelet covariance transform works its way along the profile, comparing each data point to the others separately, the PBL depths it detects must fall on the same intervals as the original data; a low-resolution profile returns blocky, low-resolution PBLs. By contrast, the curve-fitting routine detects PBL depths based on the overall shape of the profile and is therefore free to return heights between the profile's data points. For intercomparison between instruments, this property eliminates aliasing caused by the differing height intervals of the profiling data. For PBL depths from a single instrument with high temporal resolution, it returns PBL depths with realistic rates of change and development that better match the shape of the contour in lidar backscatter or virtual potential temperature.

## 6. Summary

The two main techniques for gradient-based PBL detection, wavelet covariance (Davis et al., 2000; Brooks, 2003) and simulated annealing (Steyn et al., 1999; Hägeli et al., 2000) have complementary strengths and weaknesses, as do different measurement types. The former technique is flexible and simple enough to automate for analyses of long time series and multiple sites, while the latter compensates for noisy signals and low vertical resolution. Both are applicable to the aerosol gradient approximated by lidar backscatter and also the gradient of potential temperature ( $\theta_v$ ) found in thermodynamic profiles. Used together, they make it possible to detect the PBL depth in radiosonde, lidar and infrared spectrometer profiles from the same location and to compare the resulting PBL products. An algorithm combining the two approaches was developed and applied to MPL backscatter, AERI  $\theta_v$  and radiosonde profile data measured at the Southern Great Plains site over the period of 1996–2004. Intercomparison between AERI- and radiosonde-derived PBL depths shows that the combined algorithm can partly overcome the limitations of the low AERI vertical resolution, with two-thirds of the variation explained by the regression. AERI-derived PBLs are unreliable in cloudy conditions.

The intercomparison between MPL- and radiosonde-derived PBL depths is divided into subsets based on cloud conditions and temporal cycling. The algorithm is able to detect the PBL to approximately equal agreement with radiosonde results whether clouds are present or not: in both cases, while there is considerable scatter in the intercomparison, regression  $R^2$  values are above 0.5 and the systematic error is low. MPL-derived PBL depths are most reliable during times of day when the boundary layer is mature, especially late afternoon, but least reliable during times of transition after dawn and dusk. Summertime PBL results are in greater disagreement between backscatter and thermodynamic profiles because deep convection introduces ambiguity to the thermodynamic PBL definition. MPL-derived results correctly follow the typical cloud base heights in summer, while radiosonde-derived results may be too high. MPL is unable to detect PBLs shallower than 600 m, the overlap range limit.

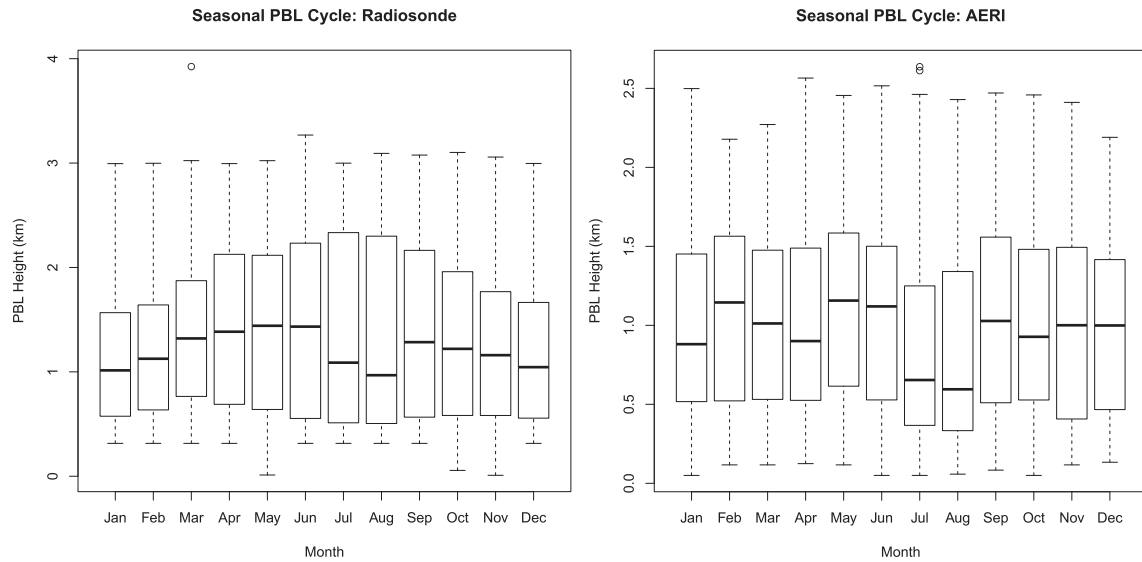


Fig. 14. Boxplots for the monthly distribution of PBL depths from radiosonde and AERI, with shallow PBLs included.

For the intercomparison between AERI- and radiosonde-derived PBL depths, the results are more complicated. The regression of the full set of PBL results is encouraging, with an  $R^2$  value of 0.67. However, the cluster of comparison points in which the AERI-derived PBL depth is much lower than the radiosonde-derived PBL depth from the same launch time becomes more significant when the results are broken down by time of day and season. The diurnal cycle of the AERI-derived PBL depth is weak but present when shallow PBLs are included in the analysis, but the seasonal cycle is not resolvable. AERI-derived PBL depths are much too shallow during the summer months, at the same time that radiosonde-derived PBL depths are wildly variable and MPL-derived PBL depths stay close to the typical cloud base depth. The greater sensitivity of the AERI instrument at lower levels may be responsible.

Both remote sensing instruments have promising, and complementary, results compared to radiosonde. MPL and AERI-derived PBL depths can therefore be considered accurate at temporal resolutions much higher than the four times daily radiosonde launch, and high-resolution PBL depths may be used for data assimilation and modeling. The detected PBL-to-free-tropospheric transition depths are not reliable, but the more detailed view of diurnal cycling in the PBL is useful in studies of aerosol transport and cloud–aerosol interactions.

#### Acknowledgments

Data were obtained from the Atmospheric Radiation Measurement (ARM) Program sponsored by the U.S. Department of Energy, Office of Science, Office of Biological and Environmental Research, Climate and Environmental Sciences Division. The authors gratefully acknowledge early discussions with Dr. Ellsworth Judd Welton of NASA/GSFC, and the funding supports of the National Basic Research Program (2013CB955804), DOE's Atmospheric System Research (ER65319), and National Science Foundation (1118325).

#### References

- Amiridis, V., et al., 2007. Aerosol lidar observations and model calculations of the planetary boundary layer evolution over Greece, during the March 2006 total solar eclipse. *Atmos. Chem. Phys.* 7, 6181–6189.
- Beyrich, F., Görsdorf, U., 1995. Composing the diurnal cycle of mixing height from simultaneous sodar and wind profiler measurements. *Bound.-Layer Meteor.* 76, 387–394.
- Bianco, L., Wilczak, J.M., 2002. Convective boundary layer depth: improved measurement by Doppler radar wind profiler using fuzzy logic methods. *J. Atmos. Ocean. Technol.* 19, 1745–1758.
- Brooks, Ian M., 2003. Finding boundary layer top: application of a wavelet covariance transform to lidar backscatter profiles. *J. Atmos. Ocean. Technol.* 20, 1092–1105.
- Davis, K.J., et al., 2000. An objective method for deriving atmospheric structure from airborne lidar observations. *J. Atmos. Ocean. Technol.* 17, 1455–1468.
- Ding, A., et al., 2009. Transport of north China air pollution by midlatitude cyclones: case study of aircraft measurements in summer 2007. *J. Geophys. Res.* 114. <http://dx.doi.org/10.1029/2009JD012339>.
- Donnell, E.A., Fish, D.J., Dicks, E.M., 2001. Mechanisms for pollutant transport between the boundary layer and the free troposphere. *J. Geophys. Res.* 106, 7847–7856.
- Feltz, W.F., et al., 1998. Meteorological applications of temperature and water vapor retrievals from the ground-based atmospheric emitted radiance interferometer (AERI). *J. Appl. Meteor.* 37, 857–875.
- Feltz, W.F., et al., 2003. Near-continuous profiling of temperature, moisture, and atmospheric stability using the atmospheric emitted radiance interferometer (AERI). *J. Appl. Meteor.* 42, 584–597.

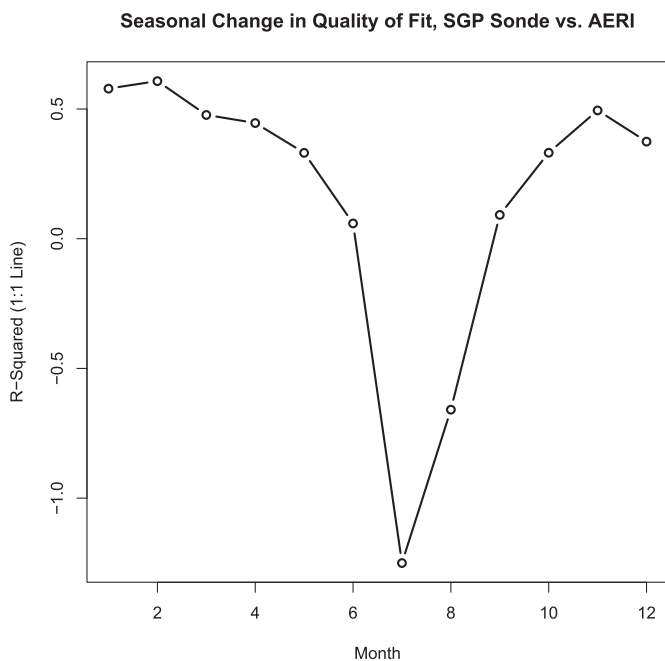


Fig. 15.  $R^2$  values assessing the quality of fit to the 1:1 line for radiosonde vs. AERI, shallow PBL depths included.

- Hägeli, P., Steyn, D.G., Strawbridge, K.B., 2000. Spatial and temporal variability of mixed-layer depth and entrainment zone thickness. *Bound.-Layer Meteor.* 97, 47–71.
- Henne, S., et al., 2004. Quantification of topographic venting of boundary layer air to the free troposphere. *Atmos. Chem. Phys.* 4, 497–509.
- Liu, S., Liang, X.-Z., 2010. Observed diurnal cycle climatology of planetary boundary layer height. *J. Clim.* 23, 5790–5809.
- Ma, M., et al., 2011. Characteristics and numerical simulations of extremely large atmospheric boundary-layer heights over an arid region in north-west China. *Bound.-Layer Meteor.* 140. <http://dx.doi.org/10.1007/s10546-011-9608-2>.
- Medeiros, B., Hall, A., Stevens, B., 2005. What controls the mean depth of the PBL? *J. Clim.* 18, 3157–3172.
- Melfi, S.H., et al., 1985. Lidar observations of vertically organized convection in the planetary boundary layer over the ocean. *J. Clim. Appl. Meteor.* 24, 806–821.
- Palm, S., et al., 1998. Inference of marine atmospheric boundary layer moisture and temperature structure using airborne lidar and infrared radiometer data. *J. Appl. Meteor.* 37, 308–324.
- Parikh, N.C., Parikh, J.A., 2002. Systematic tracking of boundary layer aerosols with laser radar. *Opt. Laser Technol.* 34, 177–185.
- Press, W.H., Teukolsky, S.A., Vetterling, W.T., Flannery, B.R., 1992. *Numerical Recipes in FORTRAN: the Art of Scientific Computing*, second ed. Cambridge University Press, pp. 436–447.
- Seibert, P., et al., 2000. Review and intercomparison of operational methods for the determination of the mixing height. *Atmos. Environ.* 34, 1001–1027.
- Seinfeld, John H., Pandis, Spyros N., 2006. *Atmospheric Chemistry and Physics: From Air Pollution to Climate Change*, second ed. WileyBlackwell, Hoboken, NJ.
- Steyn, D.G., Baldi, M., Hoff, R.M., 1999. The detection of mixed layer depth and entrainment zone thickness from lidar backscatter profiles. *J. Atmos. Ocean. Technol.* 16, 953–959.
- Stull, Ronald B., 1988. *An Introduction to Boundary Layer Meteorology*. Springer-Verlag, New York, LLC.
- Twohy, C.H., et al., 2002. Deep convection as a source of new particles in the midlatitude upper troposphere. *J. Geophys. Res.* 107, D21. <http://dx.doi.org/10.1029/2001JD000323>.